Diffusion Through Ordered Force Fields in Nanopores Represented by Smoluchowski Equation

Fu Yang Wang, Zhong Hua Zhu, and Victor Rudolph
Div. of Chemical Engineering, School of Engineering, The University of Queensland, Brisbane, QLD 4072, Australia

DOI 10.1002/aic.11747
Published online April 20, 2009 in Wiley InterScience (www.interscience.wiley.com).

The classical Einstein or Fick diffusion equation was developed in random force fields. When the equation is applied to gas transport through coal, significant discrepancies are observed between experimental and simulation results. The explanation may be that the random force field assumption is violated. In this article, we analyze molecular transport driven by both random and ordered (directional) forces in nanopores. When applied to CO_2 transport through cone-shaped carbon nano-tubes (CNTs) and Li^+ doped graphite pores, computational results show that directional force fields may significantly affect porous media flow. Directional forces may be generated by potential gradients arising from a range of non-uniform characteristics, such as variations in the pore-sizes and in local surface compositions. On the basis of the simulation and experimental results, the Smoluchowski and Fokker-Planck equations, which account for the directional force fields, are recommended for diffusion through ordered force fields in nanopores. © 2009 American Institute of Chemical Engineers *AIChE J,* 55: 1325–1337, 2009

Keywords: adsorption/gas, carbon nano-tubes, coal, diffusion (micro-porous), mathematical modeling, porous media

Introduction

The widely accepted mathematical representations for the molecular transport or surface diffusion in nanopores are in the form of the Einstein diffusion equation.[1] However, these lead to significant discrepancies between experimentally measured and theoretically computed results in many practical porous media operations. For example, the classical Einstein diffusion equation predicts that the molecular density of a gas inside nanopores should converge uniformly to the boundary condition, that is, 100% recovery of gas adsorbed in the porous media can be achieved into a flush gas containing zero concentration of the adsorbed gas. Many practical examples have shown that this cannot be achieved, contradicting the model predictions. In this article, we show through theoretical analysis and numerical simulations that the Einstein diffusion equation may lead to significant errors in situations having ordered force fields. Axial potential gradients, leading to the formation of ordered force fields, arise from variations of pore sizes and surface chemical compositions. The classical Einstein diffusion equation, which assumes molecular transport in random force fields, cannot be applied to systems having significant directional forces since this violates one of the underlying assumptions.[1] On the other hand, the Smoluchowski diffusion equation and its more general form, the Fokker-Planck diffusion equation, do incorporate directional forces, and are consequently better for application to molecular transport in nanopores with pore-size and surface chemical variations.

In this article, two case studies are described, presenting computations of induced directional forces in cone-shaped CNTs and Li^+ doped slit pores, respectively, for CO_2

Correspondence concerning this article should be addressed to F. Y. Wang at f.wang@eng.uq.edu.au

transport through porous media. The significance of the directional force fields is shown by comparing results from the Einstein and Smoluchowski diffusion equations. To illustrate the practical consequences, we also analyze two simplified versions illustrative of two possible real pore situations: pores comprised of two conical CNTs joined at the narrowest part; and slit pores that have metal ions (in this case Li^+) located centrally on the pore. The simulation results show that at the equilibrium, molecular density (concentration) profiles are neither zero nor uniform within the pores, which is consistent with laboratory and industrial observations. Since variations of both pore size and functional group distribution are inevitable in practical porous media, the results demonstrate that concentration variations may exist at equilibrium within natural porous media.

In this article, we first examine the classical Einstein diffusion equation and the limitations imposed by the simplifications that it employs. Then, the experimental observations that motivate this article and require closer examination of the underlying assumptions are described. Finally, more suitable analytical representations for molecular transport in real nanopores are presented.

The Einstein one-dimensional (1D) diffusion equation is given by[1]:

$$\frac{\partial}{\partial t}f = D\frac{\partial^2}{\partial x^2}f \tag{1}$$

The initial and boundary conditions as specified by Einstein are:

$$\begin{aligned} &f(x \neq x_0, t_0) = 0 \\ &\int_{-\infty}^{+\infty} f(x, t_0)\, dx = n \end{aligned} \tag{2}$$

In Eqs. (1) and (2), f is the number of particles per unit volume, D is the coefficient of diffusion, and n is the number of particles added to the systems at $x = x_0$ and $t = t_0$. The initial and boundary conditions described by Eq. (2) can be represented as:

$$\begin{aligned} f(x, t_0) &= n\delta(x - x_0) \\ f(x_0, t) &= n\delta(t - t_0) \end{aligned} \tag{3}$$

where δ is the Dirac delta function. The unified representation of Eq. (3) is:

$$f(x, t \to t_0; x \to x_0, t) = n\delta(x - x_0)\delta(t - t_0)$$

The analytical solution of the Einstein diffusion equation described by Eqs. (1)–(3) is a Green's function given by[1]:

$$f(x, t) = \frac{n}{\sqrt{4\pi D(t - t_0)}} \exp\left[-\frac{(x - x_0)^2}{4D(t - t_0)}\right] \tag{4}$$

The diffusion model described by Eqs. (1)–(3) and the analytical solution (4) are applicable to both molecular diffusion in the bulk gas phase and surface diffusion through micro-pores since the governing equation is the same for both cases, as presented by Do.[2] We now consider a 20 mm section in an infinitely long, smooth CNT. Selected profiles of CO_2 molecular density in this section of CNT are shown in Figure 1. In the physical system, n molecules are injected in the middle of a tube ($x = x_0 = 0$) at the initial time ($t = t_0 = 0$), leading to the formation of a Dirac delta function profile at $x = 0$ and $t = 0$. This Dirac delta function is not shown in Figure 1 due to its large magnitude. The conditions for all simulations here are: temperature = 25.0°C; pressures are specified in the individual simulations, e.g., in the Einstein diffusion equation example, the pressure at two boundaries $-\infty$ and $+\infty$ are zero corresponding to zero gas density; the surface diffusion coefficient is 3.5×10^{-6} m^2/s.

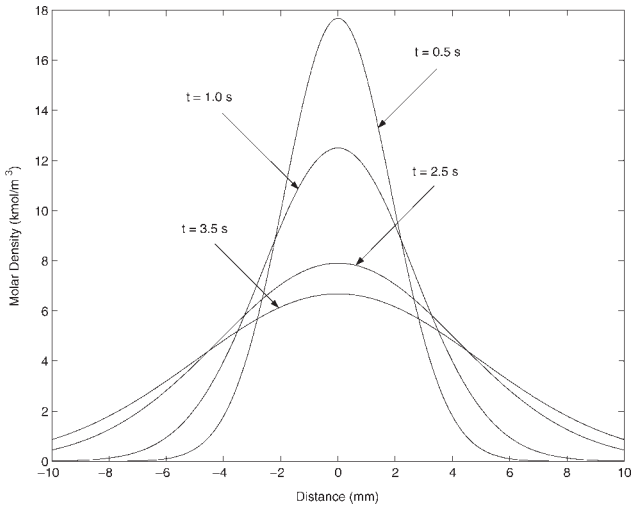

Figure 1. Profiles of CO_2 density in CNT section.

In general, we use molar densities rather than pressures inside nanopores, because there is no commonly accepted definition of pressure in small pores of Angstrom scale. The surface diffusion coefficient is about two orders of magnitude higher than CO_2 diffusivity in nanopores in activated carbons or coals with rough surfaces. This high surface diffusivity in CNTs relative to that in activated carbons and coals has been justified by Bhatia et al.[3] They argue that, in the conventional approach, complete diffuse reflection of molecules off the pore walls is assumed. However, molecular dynamics (MD) simulations have shown that wall collisions are more close to specular. Bhatia et al.[3] recommend a framework for characterizing this effect by incorporating the Maxwell coefficient, $\alpha \leq 1$, which represents a fraction of all collisions resulting in diffuse reflection, the balance being specular. The relationship between the real diffusivity, D, in CNT and the diffuse reflection diffusivity, D_{DR}, is given by:

$$D = \frac{2 - \alpha}{\alpha} D_{DR} \tag{5}$$

The parameter α represents a measure of the surface roughness with smoother surface having smaller values of α. At $\alpha = 1$, complete diffuse reflection occurs, which is the case for a porous materials with rough surfaces, such as activated carbon and coal. On the other hand, if $\alpha < 0.02$, such as might be expected in CNTs, then D could be two orders of magnitude higher than D_{DR} from which we obtain the diffusivity estimate

of 3.5×10^{-6} m^2/s. Note that the surface diffusivity of CO_2 in a CNT is a function of temperature, pore size and gas density. The determination of gas diffusivities in nano-tubes and these dependencies have been reported.[4] However, the surface diffusivity may be treated as a constant under certain conditions,[4,5] such as low gas loadings and narrow pore size variations.

Despite the extensive applications of the analytical solution given by Eq. (4), a fundamental flaw known as the "causality problem" has been identified and discussed in detail in the literature by Aranovich and Donohue.[6] It can be described as: at a finite time t, there is non-zero $f(x,t)$ at any x as shown in Figure 1. This implies that molecules can diffuse with infinite speed. In addition to the causality problem, another problem observed is that the solution of $f(x,t)$ shown in Eq. (4) and Figure 1 uniformly converges towards a boundary condition of zero as time increases. Figure 1 only shows the truncated profiles for time up to 3.5 s, and x in the interval of [-10 mm to $+10$ mm] rather than [$-\infty$ to $+\infty$], but the trend is clear. The implication is that 100% recovery of the adsorbed gas will eventually be achieved through desorption-diffusion. This conflicts with practical experience in porous media operations. For example, even under the best circumstance, coal-bed methane (CBM) recovery is typically only 50–60% without special interventions.[7] Further, stable uneven distribution of adsorbed gases is often observed in both laboratory experiments and industrial operations.[8] These discrepancies related to the recovery rate and uniformity between observation and model predictions still remain as an unsolved problem, which is addressed in this article.

Experimental Observation and Research Motivation

This study was motivated by discrepancies observed between model predictions and experimental measurements for enhanced coal bed methane (ECBM) operations. For this we use a high pressure, true tri-axial stress coal permeameter (TTSCP) explained in our previous publications.[7,8] In the TTSCP, a variety of fluids may be made to flow through a cubical porous specimen under closely controlled pressure conditions, while the specimen is subject to three independently-set, mutually-orthogonal external compressive stresses. The normal maximum operating pore pressure in TTSCP is 14 MPa, which replicates underground CBM gas pressures at about 1400 m depth. A variety of coal specimen sizes can be accommodated in the apparatus up to the maximum size of 200 mm (side length) cube. Cubic samples have the advantage that they can be rotated, permitting the permeability to be measured in three orthogonal directions. The three-dimensional (3D) strain changes are measured using the strain gages imbedded in the coal specimen. When conducting sequential core floods, the exit gas phase composition is accurately measured using a gas chromatograph (GC).

The coal specimen size used for this work was an 80 mm cube cut in general alignment with the bedding plane and the cleat directions. The two-dimensional (2D) view of an element of the coal specimen is schematically shown in Figure 2. The characteristics of the coal specimen are provided as follows.[7,8] The average distance between two fractures for the 80 mm sample is 18 mm. Porosity in coal is composed

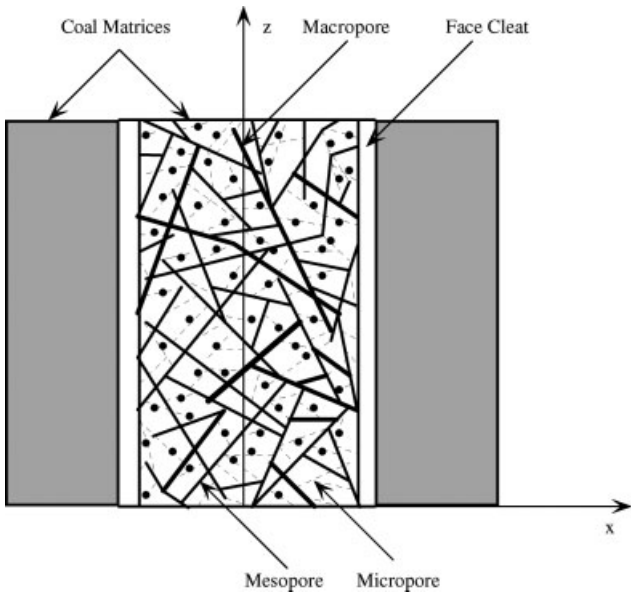

Figure 2. 2D view of an element in coal specimen.

of micro-pores (5 Å–20 Å), meso-pores (20 Å–500 Å), macro-pores (500 Å–0.1 μm), and cleats ($\sim$0.1 μm–2 mm). The mean cleat aperture in the coal specimen is inferred by indirect measurement to be 110 μm (unstressed sample), which is slightly higher than the most frequently measured cleat aperture range of 0.1–50 μm for stressed samples as reported in the literature. The total porosity of a coal is a strong and nonlinear function of the rank of coal measured by carbon content, and may vary from 4 to 18%. For high rank coals, the total porosity is typically in the range of 4–8%. We adopt the following ratios for various pore types: cleats: 1–5%; macro-pores: 10–15%; meso-pores: 5%; and micro-pores: 70–80% of total pore volume.

Two kinds of mathematical models, namely a generalized model for mass transfer in coal seams, and a simplified model, have been reported by the authors.[7,8] The parameters in these models are obtained by independent measurements, but these require some fitting adjustments to achieve satisfactory matches between the model and the experiments. The physical reasons for the necessity of parameter adjustments are explored here.

First, we describe the conventional model equation and its limitations. It was previously shown[7] that under certain operational conditions, the 2D mass transfer equations based on Figure 2 can be approximated by two sets of (1D) equations to simplify the numerical analysis. The original conceptual 1D diffusion-convection model is represented by the following two equivalent equations for multi-component systems:

$$\frac{\partial C_i}{\partial t} = \frac{D_{ei}}{\tau_D}\frac{\partial^2 C_i}{\partial x^2} - \frac{KC_i}{\tau_C \mu_m \lambda}\frac{\partial P}{\partial x}$$
$$\frac{\partial f_i}{\partial t} = \frac{D_{ei}}{\tau_D}\frac{\partial^2 f_i}{\partial x^2} - \frac{Kf_i}{\tau_C \mu_m \lambda}\frac{\partial P}{\partial x} \quad (6)$$

where C_i, f_i and D_{ei} are the concentration, molecular number density, and effective diffusivity for the ith component,

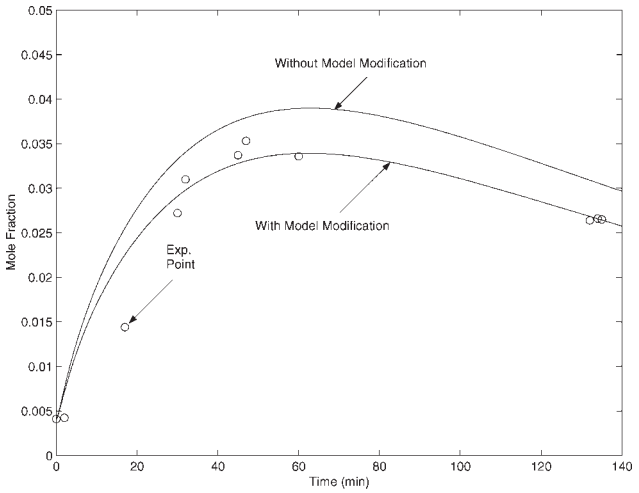

Figure 3. Dynamic responses in the second depressurization step (3100–1100 kPa).

respectively, K is the permeability, P is the gas phase pressure, λ is the half distance between two fractures, μ_m is the mean viscosity, τ_D and τ_C represent tortuosities for diffusive and convective fluxes, respectively. The use of two notations, namely mole concentration, C_i, and number density, f_i, in Eq. (6) is for notational consistency with previous articles[7,8] and Einstein,[1] respectively. Through a comparative study between experimental and simulation results using Eq. (6), the following problems have been identified.

1. In a constant pressure operation to replace adsorbed CH_4 by He under 5100 kPa, only 63% CH_4 recovery of the originally adsorbed gas (OAG) can be achieved in 72 h. When the pressure was reduced from 5100 to 3100 kPa, the mass balance shows that 82% recovery of OAG is achieved in 25 h. A second step of depressurization, from 3100 to 1100 kPa, reduces the CH_4 residual to 6% in 47 h, thereby increasing overall recovery to 94% of OAG. In all of these three operations, no significant increase in recovery rate can be achieved after certain length of time. Even if the operation time is extended to 2 weeks, a non-trivial amount of CH_4 still remains in the coal specimens. In contrast to experiments, simulations show much faster dynamics even in the zones with small driving forces. For example, simulation results suggest the reduction in residual level of CH_4 from 18 to 6% in the second depressurization step should happen within 24 h, rather than 47 h as measured experimentally. The major difference is observed where the residual level is below 8%. The simulations also indicate that at 1100 kPa, complete CH_4 recovery should be achievable in a reasonable time, which does not correspond with laboratory or field experience.

2. The shapes and magnitudes of the dynamic response curves are different from the model. Figures 3 and 4 shows the mole fraction of CH_4 in the exit gas in the second and third steps of depressurization, in which the gas pressure was reduced from 3100 to 1100 and from 1100 to 200 kPa, respectively. The uncorrected simulations are higher and have a wider distribution than the measured points, indicating that the model predicts faster and more complete residual desorption from the coal matrix than is observed in experiment.

In our previous work,[7,8] we adjusted two parameters to improve the model fit to the experimental dynamic behavior. These were the tortuosity, τ_D, and permeability, K, in Eq. (6). This achieved certain success, but some disagreements between observed and computed outcomes remain. For example, from Eq. (6) as the pressure gradient $\partial P/\partial x$ approaches zero, with finite concentration gradient $\partial C_i/\partial x$, diffusion continues due to non-zero diffusivity. Consequently, the model predicts a finite diffusion flux until $\partial C_i/\partial x$ vanishes, which implies that the complete recovery is achievable if the concentration of the component is kept at zero at the boundaries. This contradicts observations that there can be unrecoverable adsorbed material. On the basis of these facts, we conclude that the conventional model structure requires modification because adjusting the parameter values (while necessary) cannot alone fix these issues.

Figures 3 and 4 show that the conventional model always over-estimates the mass transfer rates from coal matrices to their environments. This implies that an additional force acting on the gas molecules opposing their diffusion and slowing the release dynamics. To account for this, an additional convection flux with a pseudo velocity q_i for the ith component, the possible origins of which will be explained later, is introduced as follows:

$$\frac{\partial C_i}{\partial t} = \frac{D_{ei}}{\tau_D}\frac{\partial^2 C_i}{\partial x^2} - \frac{KC_i}{\tau_C \mu_m \lambda}\frac{\partial P}{\partial x} + q_i \frac{\partial C_i}{\partial x}$$
$$\frac{\partial f_i}{\partial t} = \frac{D_{ei}}{\tau_D}\frac{\partial^2 f_i}{\partial x^2} - \frac{Kf_i}{\tau_C \mu_m \lambda}\frac{\partial P}{\partial x} + q_i \frac{\partial f_i}{\partial x} \tag{7}$$

A better fit of the simulation to the data is obtained using Eq. (7) instead of Eq. (6). The value of q_i is found from:

$$q_i = \alpha \frac{KC_i}{R_g T \tau_C \mu_m \lambda} = \alpha \frac{Kf_i}{R_g k_A T \tau_C \mu_m \lambda} \tag{8}$$
$$\alpha = 0.13 \text{ to } 0.14$$

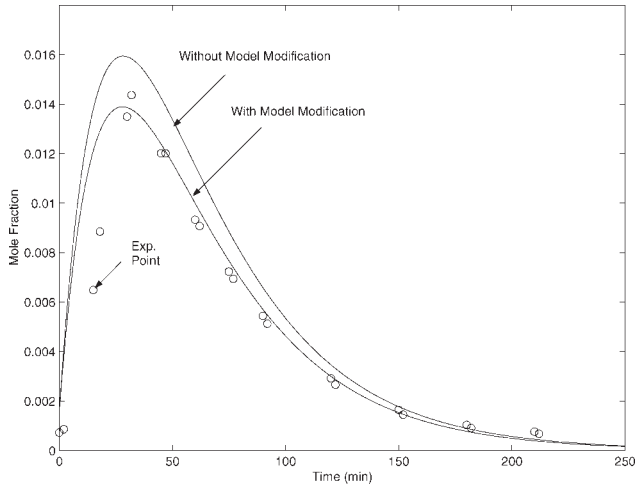

Figure 4. Dynamic responses in the third depressurization step (1100–200 kPa).

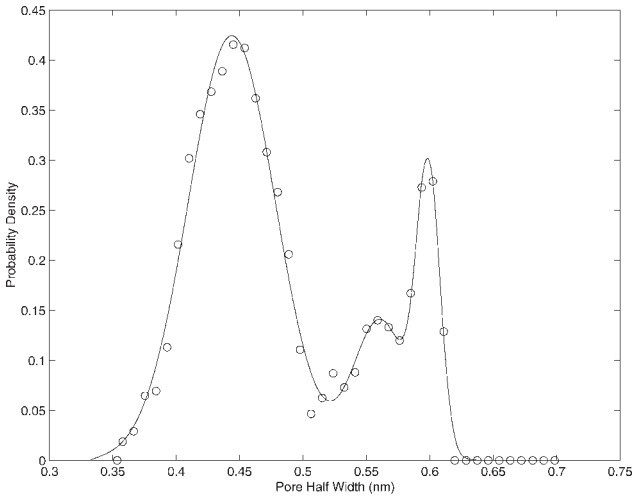

Figure 5. Nanopore size distribution of a coal specimen.

where R_g is the ideal gas constant, k_A is the Avogadro constant, and α is an empirical constant determined from backfitting the experimental data. The simulation results using Eqs. (7) and (8) are also depicted in Figures 3 and 4, and show a significantly improved fit with the experimental data for both depressurization stages.

Importantly, incorporating q_i allows for the situation where there is no gas flux even though a finite concentration driving force $\partial C_i/\partial x$ may still exist. This corresponds to observations that complete gas recovery cannot be achieved even for very long operational times.

We now seek to explain the source of the additional convection flux term $q_i \partial C_i/\partial x$. Coals are highly heterogeneous materials with very complex morphology, and the term is ascribed to the non-uniform nature of the porosity, elaborated further below. As an example, the nanopore size distribution curve for a coal specimen is presented in Figure 5, (from data reported by Bae and Bhatia[9]) showing a complex multi-modal pattern.

Smoluchowski Diffusion Equation

The Einstein diffusion equation is derived for molecules moving under random forces without influences from directional force fields. We hypothesize that the additional convection flux term comes about because the molecules in nanopores move under both random and ordered forces. Consequently, the diffusion equation should account for the effects from directional force fields. The development of the Fokker-Planck and Smoluchowski diffusion equations presented below follows methods provided in the lectures conducted by Schulten and Kosztin[10] at the University of Illinois at Urbana-Champaign. Since this mathematical procedure has not been systematically described in classical chemical engineering textbooks, it is introduced briefly in this section.

We start from Langevin equation given by:

$$m\ddot{\mathbf{x}} = -\gamma\dot{\mathbf{x}} + \mathbf{F}(\mathbf{x}) + \sigma E(t)$$
$$\mathbf{x} = \begin{bmatrix} x_1 \\ x_2 \\ \vdots \\ x_N \end{bmatrix}; \quad \mathbf{F} = \begin{bmatrix} F_1(\mathbf{x}) \\ F_2(\mathbf{x}) \\ \vdots \\ F_N(\mathbf{x}) \end{bmatrix} \tag{9}$$

In Eq. (9), we assume that there are N molecules in the system; $x_1, \ldots, x_N$ and $F_1, \ldots, F_N$ represent the positions and directional forces for individual molecules numbered from 1 to N, respectively; $\mathbf{x}$ and $\mathbf{F}$ are vectors describing the positions of molecules and directional forces acting on the molecules, respectively; E is the random force, m is the mass of molecules; γ and σ are the frictional coefficient and amplitude of the random fluctuating force, respectively. With the assumption that:

$$|\gamma\dot{\mathbf{x}}| >> |m\ddot{\mathbf{x}}| \tag{10}$$

the following Fokker-Planck diffusion equation can be developed:

$$\frac{\partial}{\partial t} f = \left(\nabla^2 D - \nabla \cdot \frac{\mathbf{F}}{\gamma} \right) f$$
$$\mathbf{D} = \frac{\sigma^2}{2\gamma^2} \tag{11}$$

If we further assume that the force field can be related to a scalar potential given by:

$$\mathbf{F}(\mathbf{x}) = -\nabla U(\mathbf{x}) \tag{12}$$

the Fokker-Planck diffusion equation described by Eq. (11) can be converted to the Smoluchowski diffusion equation described as:

$$\frac{\partial}{\partial t} f = \nabla \cdot [D(\nabla - \beta\mathbf{F})f]$$
$$= \nabla \cdot [D(\nabla + \beta\nabla U)f] \tag{13}$$
$$\beta = \frac{1}{k_B T}$$

where k_B is the Boltzmann constant. The procedure for the derivation of the Smoluchowski diffusion equation from the Fokker-Planck diffusion equation is provided in Appendix A.

Equation (11) is similar to the equation for small particle transport in an external force field described by Friedlander.[11] Since the potential energies of gases in nanopores can be computed by using Lennard-Jones type potential equations, which satisfy the assumption represented by Eq. (12), the Smoluchowski diffusion equation in Eq. (13) is applicable to gas molecule transport through nanopores. From Eq. (13), it may be noted that the Einstein diffusion equation is only applicable under the following mathematical condition:

$$|\nabla f| >> |\beta(\nabla U)f| \tag{14}$$

To solve the Smoluchowski diffusion equation described by Eq. (13), it is necessary to compute the potential energy of

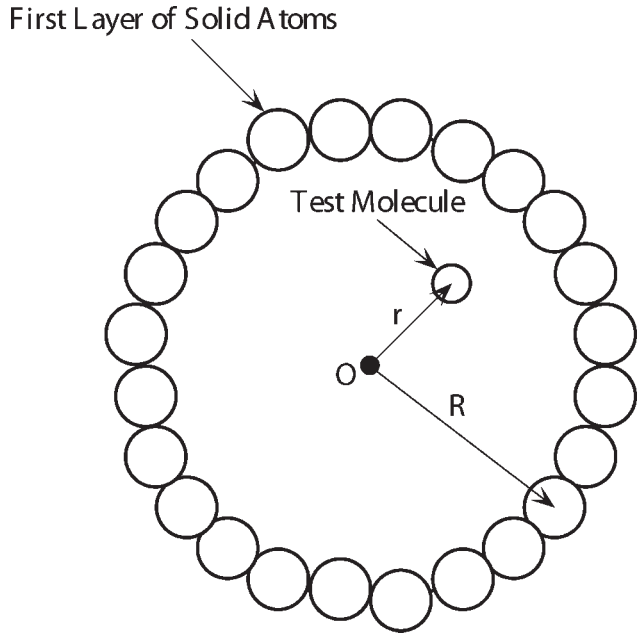

Figure 6. Cross sectional view of cylindrical pore.

molecules in nanopores. This can be done by using Lennard-Jones type potential equations for nanopores with various shapes.

Potential Energy Equations

It has been recognized that for the slit shaped pores, such as micro-pores in coals and activated carbons, the Steele 10-4-3 potential energy equation[12] provides good results. It is described as:

$$U(z,w) = \frac{5}{3}U_0\left\{\frac{2}{5}\left[\frac{\sigma_{sg}^{10}}{(w+z)^{10}} + \frac{\sigma_{sg}^{10}}{(w-z)^{10}}\right] - \left[\frac{\sigma_{sg}^{4}}{(w+z)^{4}} + \frac{\sigma_{sg}^{4}}{(w-z)^{4}}\right] - \left[\frac{\sigma_{sg}^{4}}{3\Delta(0.61\Delta+w+z)^{3}} + \frac{\sigma_{sg}^{4}}{3\Delta(0.61\Delta+w-z)^{3}}\right]\right\}$$

$$U_0 = \frac{6}{5}\pi\rho_s\varepsilon_{sg}\sigma_{sg}^2\Delta \tag{15}$$

In Eq. (15), z is the distance from the central plane of the pore, w is the half width of slit-shaped pores, U_0 is the minimum interaction energy between a gas molecule and a single lattice layer of the adsorbent, ρ_s is the number of lattice molecules per unit volume, Δ is the spacing of lattice layers, ε_{sg} and σ_{sg} are the cross potential well depth and the effective diameter for the adsorbate-adsorbent molecule atoms. These cross parameters are calculated using the Lorentz-Berthelot rules as follows: $\varepsilon_{sg} = (\varepsilon_s\varepsilon_g)^{1/2}$, and $\sigma_{sg} = (\sigma_s+\sigma_g)/2$. The pair ($\varepsilon_s$, σ_s) and (ε_g, σ_g) are the Lennard-Jones parameters for a surface atom and a gas molecule, respectively. The Steele 10-4-3 potential energy equation described by Eq. (15) is an approximation, refer Rao et al.[13] To reduce errors induced by the approximation, the Steele 10-4-3 potential energy equation is handled by adjusting the solid-fluid interaction energy through a solid-fluid binary interaction parameter, k_{sf}, such that the experimental Henry's constant is reproduced by the MD simulations.[14,15] Thus:

$$\varepsilon_{is} = (1-k_{sf})\sqrt{\varepsilon_i\varepsilon_s} \tag{16}$$

It has been shown by Do and Do[14,15] that satisfactory results can be obtained by adjusting k_{sf} between -0.05 to 0 for CCl_4 and C_6H_6 adsorbed on the activated carbons. We have used $k_{sf} = -0.03$ for the CO_2-C systems, a minor correction which hardly affects the main results.

The cross sectional view of a cylindrical CNT is schematically shown in Figure 6, in which R is the radius from the CNT axis to the centre of the carbon molecule in the first layer, and r represents the distance from the axis to the centre of the test molecule.

The potential energy equation for cylindrical pores as shown in Figure 6 has been developed by Zhang et al.[16] as:

$$U = \pi^2\rho_s\sigma_{sg}\varepsilon_{sg}\left\{\frac{7}{32}\frac{1}{R^9\left[1-(r/R)^2\right]^9}F\left[-\frac{9}{2},-\frac{7}{2};1;\left(\frac{r}{R}\right)^2\right] \times \frac{1}{R^3\left[1-(r/R)^2\right]^3}F\left[-\frac{3}{2},-\frac{1}{2};1;\left(\frac{r}{R}\right)^2\right]\right\} \tag{17}$$

The gamma function representation of the hypergeometric function $F(a, b; c; \zeta)$ in Eq. (17) is given by:

$$F(a,b;c;\zeta) = \frac{\Gamma(c)}{\Gamma(b)\Gamma(c-b)}\int_0^1 v^{b-1}(1-v)^{c-b-1}(1-v\zeta)^{-a}\,dv \tag{18}$$

There is no pore-size restriction specified in the development of Eq. (17)[16] provided that a single layer of gas molecules can be accommodated in CNTs. For our current purposes, the CNT radii, R, are greater than 3.5 Å ($D_p > 7.0$ Å), providing sufficient space for the formation of a single CO_2 layer in a CNT, and consequently allowing the application of Eq. (17).

From Eqs. (15) and (17), it can be observed that the potential energies of molecules in both slit and cylindrical shaped pores are very sensitive to the pore sizes (w and R for the slit and cylindrical shaped pores, respectively). Potential profiles for CO_2 molecules in cylindrical CNTs with various pore sizes are shown in Figure B1 in Appendix B. The adsorption energy is defined as the negative of the minimal potential energy. The profiles of the adsorption energies provide indications of potential field characteristics. The adsorption energy profiles for three gases, namely CO_2, CH_4, and N_2, are shown in Figure B2 in Appendix B. From Figures B1 and B2, it can be seen that in certain pore size range, potential energies change dramatically with pore size. Clearly, if the pore size in a porous material is not uniform, there may be significant directional forces on the molecules induced by the pore size variation.

Solution of Smoluchowski Diffusion Equation

Diffusion in linear potential fields

The Smoluchowski diffusion equation given by Eq. (13), and the Fokker-Planck Eq. (11), can be solved numerically by using the orthogonal collocation on finite element method,[8] or other discretization techniques. However, an analytical solution can be developed with the following two assumptions: (1) the diffusivity D is not a strong function of the position x; and (2) the potential function can be approximately represented by a linear function of position, that is, $U(x) = cx$. It will be demonstrated later that for CO_2 transport through CNTs under low pressure, these two assumptions can be supported. In this case, the Smoluchowski diffusion equation is simplified to the following linear partial differential equation:

$$\begin{aligned} &\frac{\partial}{\partial t}f = D\frac{\partial^2}{\partial x^2}f + q\frac{\partial}{\partial x}f \\ &q = D\beta c \end{aligned} \tag{19}$$

Using a mathematical transformation $y = x + qt$, the following partial differentiations are demonstrated:

$$\begin{aligned} &\frac{\partial f(y,t)}{\partial t} = \frac{\partial f}{\partial t} + \frac{\partial f}{\partial y}\frac{\partial y}{\partial t} = \frac{\partial f}{\partial t} + q\frac{\partial f}{\partial y} \\ &\frac{\partial f(y,t)}{\partial x} = \frac{\partial f}{\partial y}\frac{\partial y}{\partial x} = \frac{\partial f}{\partial y} \\ &\frac{\partial^2 f(y,t)}{\partial x^2} = \frac{\partial}{\partial y}\left(\frac{\partial f}{\partial y}\right)\frac{\partial y}{\partial x} = \frac{\partial^2 f}{\partial y^2} \end{aligned} \tag{20}$$

Consequently, the original diffusion equation described by Eq. (19) provides the following equivalent equation through the similarity transformation:

$$\begin{aligned} &\frac{\partial}{\partial t}f(y,t) = D\frac{\partial^2}{\partial y^2}f(y,t) \\ &y = x + qt \end{aligned} \tag{21}$$

Since after the similarity transformation, the Smoluchowski diffusion equation follows the format of the Einstein diffusion equation, the analytical solution originally developed by Einstein applies:

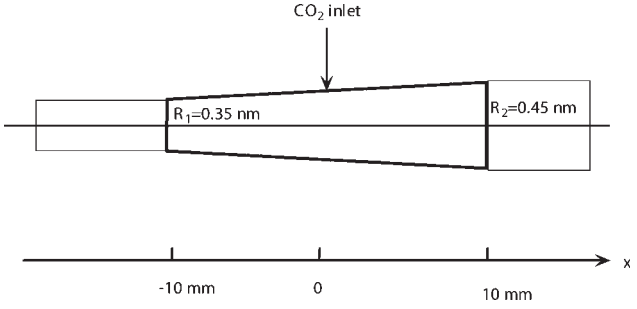

Figure 7. Schematic diagram of cone-shaped CNT.

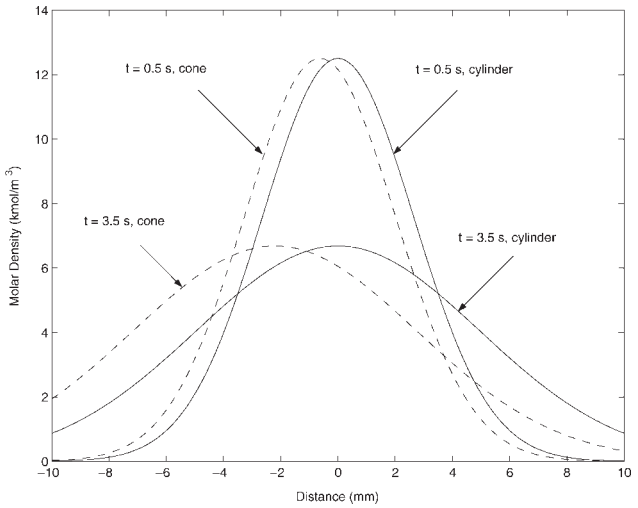

Figure 8. Profiles of CO_2 densities in conical and cylindrical CNTs.

$$\begin{aligned} f(y,t) &= \frac{n}{\sqrt{4\pi D(t-t_0)}}\exp\left[-\frac{(y-y_0)^2}{4D(t-t_0)}\right] \\ f(x,t) &= \frac{n}{\sqrt{4\pi D(t-t_0)}}\exp\left[-\frac{[(x+qt)-(x_0+qt_0)]^2}{4D(t-t_0)}\right] \end{aligned} \tag{22}$$

This analytical solution will be used to examine two practical examples.

Potential gradient induced by pore size variations

Since the potential energy is a strong function of pore size for both slit and cylindrical shaped pores as shown by Eqs. (15) and (17), directional forces will be induced by pore size variations. We use a cone-shaped pore as an example to show the main outcomes related to the diffusion process. The example CNT is shown schematically in Figure 7. The length of the tube is 20 mm. The radii at two ends are 0.35 and 0.45 nm, respectively, based on the nanopore size distribution in Figure 5, which shows that a significant portion of nanopores ($\sim$35%) in the coal specimen occurs in this size range. CO_2 is used as the test gas. To use the analytical solution given by Eq. (22), we assume that the potential gradient extends linearly beyond this section of CNT. If a numerical solution technique is used, arbitrary end boundaries can be used and more general systems can be investigated.

The potential energy distribution along the axial direction of CNT can be computed by using Eq. (17). It shows that the assumption of linear potential field is acceptable.

At temperature $T = 298.16$ K, the constant q is computed as $q = 6.31 \times 10^{-4}$ m/s using Eq. (19). Selected profiles of CO_2 densities in conical and cylindrical shaped CNTs at two different times are shown in Figure 8.

The CO_2 profiles are symmetrical in the cylindrical pores, but CO_2 molecules favor the small side in cone-shaped pores. In a ''bow tie'' shaped CNT (two cones joined at the small sides of the cones, Figure 14), 100% desorption of

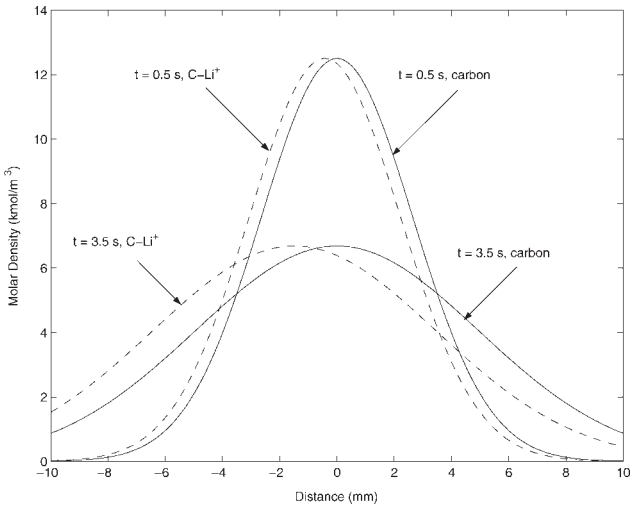

Figure 9. Profiles of CO_2 densities in slit shaped C-Li^+ pore and pure CNT.

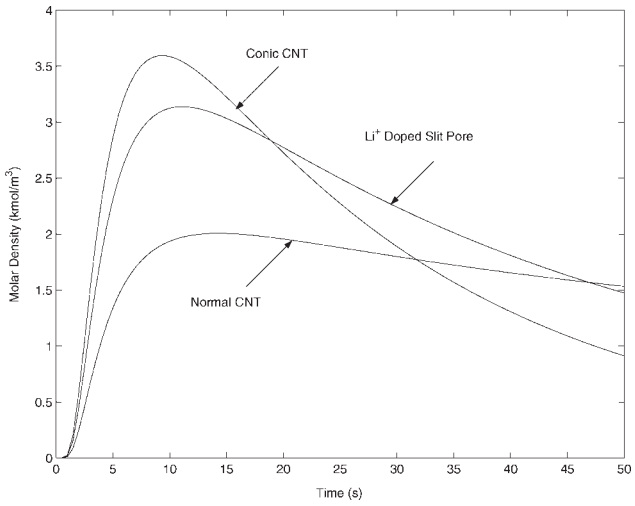

Figure 10. Molar density profiles at x = –10 mm.

CO_2 will not occur even if the open (large) ends are held indefinitely at zero CO_2 concentration.

Potential gradient induced by chemical component variations

It is well known that functional groups and metal ions on carbon surfaces significantly affect adsorption characteristics. As an example, we examine CO_2 adsorption in slit-shaped carbon pores doped with Li^+. The adsorption energies of CO_2 on pure Li^+ and graphite surfaces computed by using Eq. (15) show that compared with graphite, the CO_2-Li^+ pair possess much stronger affinity. Consequently, for a doped graphite surface, if the Li^+ is not uniformly distributed, a potential energy gradient will be induced.

For simplicity, the following situation is analyzed: pore size $w = 0.8$ nm; surface coverage of Li^+ varies linearly from 0.6 to 0. At this pore size, the potential energies for CO_2-Li^+ and CO_2-C systems are -24.25 and -14.20 kJ/mol, respectively. The estimated value of q (Eq. 19) is $q = 4.26 \times 10^{-4}$ m/s, which is smaller than that for the cone-shaped CNT. Profiles of CO_2 densities in slit-shaped pores with and without Li^+ ions are shown in Figure 9, for two different times. Again, it can be predicted that if the low potential (high Li^+ composition) zone is located in the middle part of a slit pore, complete CO_2 desorption cannot be accomplished even with zero CO_2 concentration at the pore mouth.

The flux induced by the directional force fields arising from size (in the cone-shaped pores) or chemical gradients (for Li^+ doped pores) induces different behavior at the opposite open ends of the pores. Figure 10 shows the CO_2 molar density profile (with time) that at $x = -10$ mm (the narrow end for CNT and highly doped end for slip pore). The maximum densities for the cone-shaped CNT and Li^+ doped slit pore are much higher than that for normal CNT but they also decay more quickly. At the opposite end of the pores at $x = +10$ mm, the opposite trends are evident, Figure 11. The directional forces induced by potential gradients on molecular transport in nanopores can be very significant as demonstrated by Figures 8–11.

Steady state solution for cone-shaped CNT

We now consider the case shown in Figure 12 for a cone-shaped CNT with the boundary conditions $f(0, t) = 0$ at $x = 0$ and a constant external flux J at $x = 10$ mm. In this case, the diffusion flux and potential induced flux are in the same direction. Steady state operation is possible, which is analyzed in this sub-section.

The flux is given by:

$$J = -D\left(\frac{\partial}{\partial x}f + \frac{\partial U}{\partial x}\beta f\right) \tag{23}$$

In the steady state, J = constant, giving the solution[11]:

$$f(x) = -\frac{J}{D}\exp(-\beta U)\int_0^x \exp[\beta U(v)]\,dv \tag{24}$$

For the CNT here, $U(v) = cv$, giving:

$$f(x) = -\frac{J}{Dc\beta}[1 - \exp(-c\beta x)] \tag{25}$$

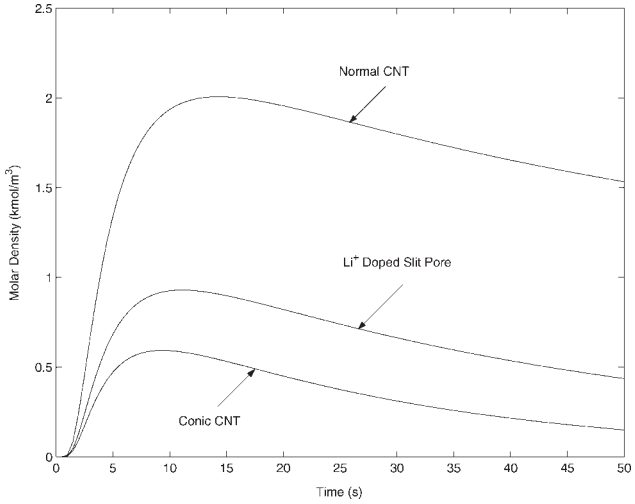

Figure 11. Molar density profiles at x = +10 mm.

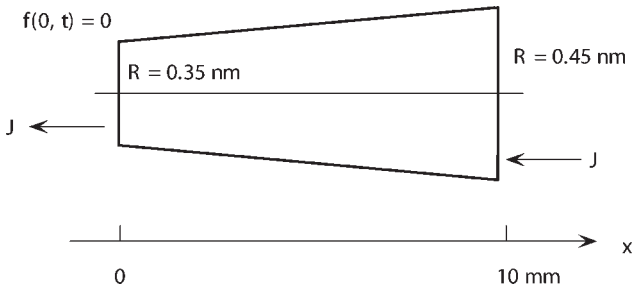

Figure 12. Cone-shaped CNT with external flux.

The value of J cannot be specified arbitrarily. The Smoluchowski diffusion equation at steady state represented by Eq. (19) with $\partial f/\partial t = 0$ describes the density profile $f(x)$ from which the flux J is obtained using Eq. (23). Equation (19) can be solved by using the orthogonal collocation method,[8] as described in next section. For the specified parameters, the molar flux is determined as $J = 0.1180$ mol/(m^2 s). The molar density profiles computed numerically and analytically using Eq. (19) with $\partial f/\partial t = 0$ and Eq. (25) are shown in Figure 13. The purpose of this example is to show that the steady state operational conditions can be readily determined for nanopores, and that directional driving forces accelerate gas flux.

Stable Adsorbed Gas in Real Systems

In this section, we examine some possible pore configurations which may explain the observations that some gas remains apparently stably and permanently adsorbed in coal despite a concentration gradient that supports desorption. Two pore arrangements are presented, representing idealized versions of what may actually be the physical mechanism in real coal, which prevent 100% release of adsorbed CO_2 in a conventional desorption processes. These two configurations are double cone ("bow-tie") shaped CNTs and Li^+ doped CNTs, with the Li^+ ions predominantly located at the central part of the tube, Figure 14.

The CNTs shown in Figure 14, taken to be initially filled with CO_2 molecules, are placed in a Helium environment

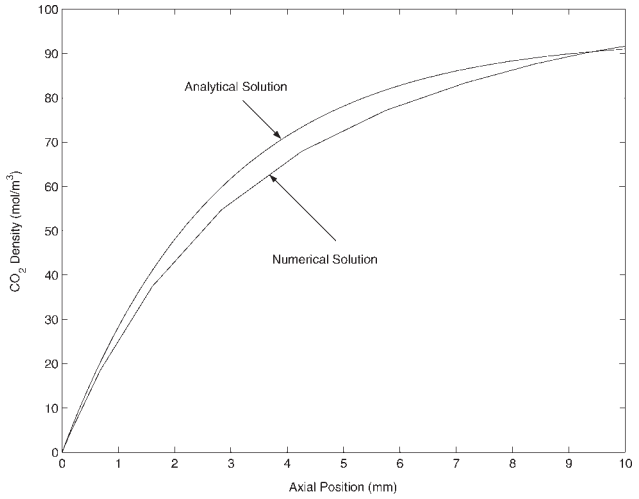

Figure 13. Steady state solutions for cone-shaped CNT.

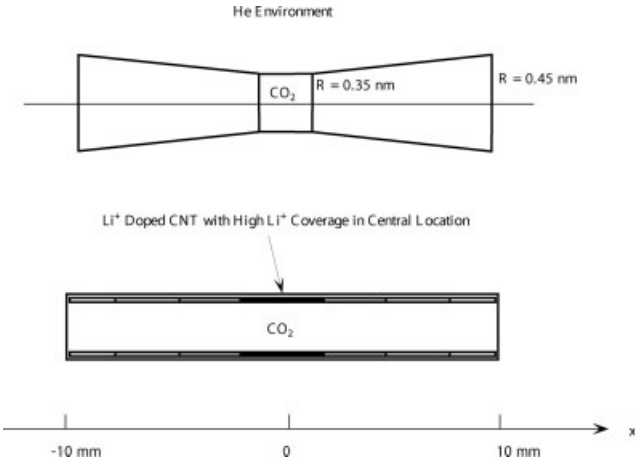

Figure 14. Arrangements that retain elevated adsorbed concentrations inside the pore.

and the tubes allowed to empty of CO_2 due to desorption and diffusion. On the basis of Eq. (1), all the CO_2 should be released provided that a long enough time is allowed. However, Eq. (13) (for general cases) and Eq. (19) (for the particular CNT examples here) show that the release will stop under the following limitation:

$$\begin{aligned} \nabla \cdot [D(\nabla + \beta \nabla U)f] &= 0, \quad \text{in general} \\ D\frac{\partial^2}{\partial x^2} f \; + \; q\frac{\partial}{\partial x} f &= 0, \quad \text{for case studies} \end{aligned} \tag{26}$$

Equation (26) can be solved by using the orthogonal collocation method as follows:

$$\frac{D}{L^2}\mathbf{Bf} + \frac{q}{L}\mathbf{Af} = \begin{bmatrix} 0 \\ \vdots \\ 0 \end{bmatrix}; \quad \mathbf{f} = \begin{bmatrix} f_1 \\ \vdots \\ f_M \end{bmatrix} \tag{27}$$

where $\mathbf{A}$ and $\mathbf{B}$ are orthogonal collocation matrices for the first and second order spatial derivatives, respectively, L is the half length of the CNT ($L = 10$ mm $= 0.01$ m in case studies), the subscripts 1 to M specify the spatial position of f, and M is the total number of collocation points. The computational methods for the determination of the matrices $\mathbf{A}$ and $\mathbf{B}$ are provided by Villadsen and Michelsen[17] and Finlayson[18] who also supply FORTRAN solution codes.

Equation (26) is solved with appropriate boundary conditions for the double cone-shaped CNT, using $D = 3.5 \times 10^{-6}$ m^2/s and $q = 1.26 \times 10^{-3}$ m/s. The molar density profile is shown in Figure 15, which shows that a CO_2 density profile exists in the tube at equilibrium, even when the CO_2 concentration is zero at the open ends. Consequently, some CO_2 remains in the CNT and cannot be drained. The equilibrium curve for the Li^+ doped CNT is similar to Figure 15 but is slightly less pronounced due to a slightly smaller value of q (8.52×10^{-4} m/s) than in the double cone-shaped CNT (1.26×10^{-3} m/s). The equilibrium arises because there are two opposing driving forces, namely the concentration gradient induced driving force pushing CO_2 out of the CNT, and the potential gradient induced directional force pulling CO_2 into the middle section.

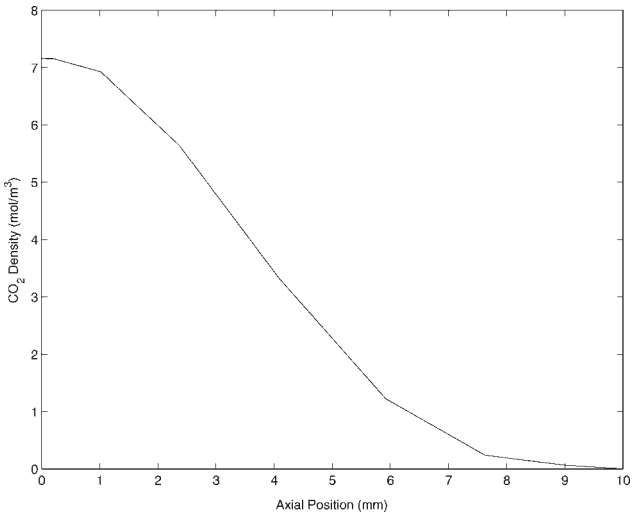

Figure 15. Equilibrium CO_2 density profile in double cone-shaped CNT.

Dynamic Changes to Model Parameters

A close examination of Figures 3 and 4 reveals differences between experimental and simulation results even using the modified model with the additional convection flux, as developed above. The main deviations can be identified as follows: (1) the modified model predicts the later stages of the depressurization operations reasonably well, but fails to predict the time delays in the early depressurization stages for both cases; and (2) in the third depressurization operation shown in Figure 4, the modified models under predict the mole fraction in the gas phase in the later stage ($t > 200$ min.). Consequently, the model requires further refinement to improve the match with experiment.

These issues can be numerically addressed by dynamically varying the nanopore permeability and parameter q_i. Both changes can be physical justified. In this version of the model, a smaller nanopore permeability with lower pore connectivity (larger nanopore tortuosity), and a larger q_i value, are used in the early stage. The permeability is then progressively increased and the value of q_i reduced, until they reach their ultimate constant values. This is a development of a strategy for solving molecular transport in nanopores with broad pore-size distribution.[4] We use a single component system for notational simplicity and consistency to previous work[4] to explain the concepts in the analysis, but note that the analysis is extendable to multi-component systems. The general definition of the permeability B_μ for nanopores is given by:

$$J_\mu = -B_\mu(P_\mu)\frac{\partial P_\mu}{\partial x} \tag{28}$$

where J_μ is the molar flux in a nanopore and P_μ is the pressure surrounding the nanopore. This is different from the conventional definition of the permeability, K, for Darcy flow represented in Eqs. (6) and (7). In the conventional definition, the permeability K is not a function of the diffusivity and tortuosity, however, in the generalized form of permeability in nanopores, the following relationship holds using the Toth isotherm[4]:

$$B_\mu(P_\mu) = \frac{\rho_p}{\tau_\mu(P_\mu)}\int_{w_{min}}^{w_{max}} D_\mu(P_\mu, w) \times \frac{\hat{\rho}(P_\mu, w)}{P_\mu}\left[1 - \frac{(b(w)P_\mu)^{t_o}}{1+(b(w)P_\mu)^{t_o}}\right] f_d(w)\, dw \tag{29}$$

where ρ_p and $\hat{\rho}$ are solid and average gas density, respectively, t_μ is the nanopore tortuosity, b and t_o are parameters in the Toth isotherm model, and f_d is the pore size distribution function. For the detailed derivation of Eq. (29), refer Wang et al.[4] The simulation results show that at very low gas densities, the permeability increases gradually, reaching a maximum, followed by gradual decrease for medium to high concentration regimes. The physical explanation for this is as follows. The higher the concentration, the less the available pore space for gas transport, and the smaller the value of $1-[(bP_\mu)^{t_o}/(1+(bP_\mu)^{t_o}]$ in Eq. (29), leading to the reduced permeability with the increase of adsorbed gas concentration.

Since our experiments were carried out in a medium concentration regime, an increase of permeability as the adsorbed gas declines seems justifiable and we have matched a time varying tortuosity τ_D in Eq. (7) to fit the experimental data. Note, however, that the permeability is extremely sensitive to the pore connectivity.[4] A rigorous computation of B_μ for coal specimens cannot be done because of the complexity and heterogeneity of coal morphology.

We also offer a justification to use a time-varying value for q_i. It is well known that adsorption and desorption induce swelling and shrinkage of porous materials.[8] One can speculate that larger pores shrink more easily than smaller ones in a desorption process due to comparatively smaller Young's modulus, leading to the reduction of the pore-size difference. Since q_i can be viewed as a measure of the material uniformity, reducing its value as pore-size variations decline seems physically reasonable. Using the adjusted parameters τ_D and q_i in Eq. (7), satisfactory fits for both depressurization processes are obtained, refer Figures 16 and 17. While these parameters are empirically determined at this time, it can be seen that they have physical meaning, could be amenable to independent measurement, and follow the anticipated trends.

It should be pointed out that the well-known Fick's diffusion equation is still widely applied to diffusion processes in nanopores with acceptable results. We attribute this success to the following factors.

1. In theoretical studies on molecular transport through CNTs using atomically detailed simulations,[3,19] a unique pore-size is assumed in each simulation although a variety of pore-sizes are investigated in different simulations. For example, this strategy was used by Bhatia et al.[3] to study pore-size effects on diffusion properties for CNTs , in which a unique pore-size is assigned to each CNT in a range of $R = 0.68$–4.05 nm. Although a number of pore-sizes were investigated in separate simulations for different CNTs, the results are insufficient for the study on mass transfer in a single CNT with a broad pore-size distribution. Further work was carried out by Bhatia's co-workers, Chan and Sholl,[19] with the same assumption on the uniqueness of the pore-size.

2. It can be observed from Figure B2 in Appendix B that energies for CO_2 and CH_4 adsorptions on CNTs are very

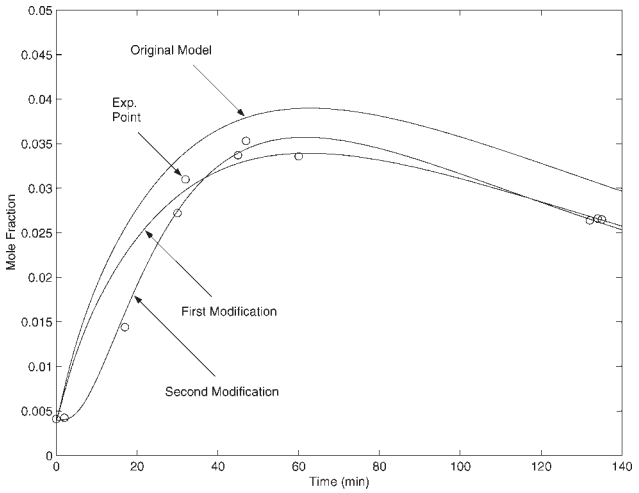

Figure 16. Modified predictions for the second depressurization step (3100–1100 kPa).

sensitive to pore-sizes in the range of $R = 0.35$–0.50 nm. The significance of the pore-size effects reduces with the increase of pore-sizes above $R = 0.5$ nm. As $R > 0.7$, the adsorption energy curves become very flat, indicating negligible direction forces induced by potential energy gradients. That is, the errors introduced by the ignorance of the directional forces could be tolerated for CNTs with relatively large but non-unique pore-sizes.

3. In the cases that both diffusive and convective mass fluxes co-exist, such as the process described by Eq. (6), the errors caused by the missing term can be compensated through the adjustment of parameters in the original convection function. However, if the pressure gradient $\partial P/\partial x$ vanishes earlier than the concentration gradient $\partial C/\partial x$, this adjustment becomes ineffective after the disappearance of $\partial P/\partial x$.

If one of these three conditions is satisfied, reasonable model prediction results can be obtained using Fick's diffusion equation (classified as Fick class). However, if these conditions are completely violated (classified as Smoluchowski class), misleading results could be obtained as shown by our experimental observations. The popularity of the Fick's diffusion equation indicates that a large number of diffusion processes can fulfill at least one of these conditions. On the other hand, the impact of directional forces incorporated in Fokker-Planck and Smoluchowski diffusion equations could be very significant for other processes with the condition violations. Although the size of the Smoluchowski class could be smaller than the Fick class with the ratio estimated as 20:80 by the authors, it consists of important practical processes as demonstrated in this work.

From a practical viewpoint, methane residual recovery generates less economical incentive compared with primary operations. Since significant improvement in methane recovery can be achieved by using ECBM operations instead of CBM technology (from 50 to 90% recovery), the significance of a further study on the field-model mismatch for the residual recovery is of limited interest to industry at the moment. Because of the fast shrinkage of energy resources, a recovery of fuel residuals may become important in the near future, which requires improved models. Consequently, a rigorous study on the Fokker-Planck and Smoluchowski diffusion equations is of both theoretical and practical significance.

Conclusions and Recommendations

This article examines the effect of potential gradient induced directional forces on molecular transport through nanopores. We draw the following conclusions.

1. The Einstein and Fick diffusion equations assume random force fields that apply to molecular transport in diffusive flow. In many real situations, this assumption may not be correct. In these cases, the Smoluchowski and Fokker-Planck diffusion equations, which account for ordered force fields, should be applied. Force fields may arise in nanopores with non-uniform pore-size and variable surface compositions. In special cases, such as linear potential fields and time-invariant boundary conditions, the Smoluchowski diffusion equation can be solved analytically through a similarity transformation. However, for systems with general potential fields and arbitrary boundary conditions, numerical methods such as the orthogonal collocation on finite elements (OCFE) method,[8] are required for solution of Smoluchowski and Fokker-Planck diffusion equations.

2. Potential fields within nanopores can be approximately characterized using the Steele 10-4-3 potential energy equation for the slit shaped pores,[12] and the 9-3 potential energy equation and hypergeometric approach developed by Zhang et al.[16] for cylindrical shaped pores. Although these two potential equations are simplified approximations to complex potential fields, satisfactory results can be obtained by incorporating a solid-fluid binary interaction parameter, k_{sf}, into the models.[4,14,15] It can be shown that for a number of widely studied gases, such as CO_2, CH_4, and N_2, the potential energy profiles can be approximately represented as piecewise linear functions of pore sizes, which simplifies analysis and computations.

3. A quantifiable equilibrium profile exists for a pore with a lower potential energy in the middle zone than in the two outer zones. This equilibrium profile is neither uniform nor trivially small, and may prevent complete desorption by

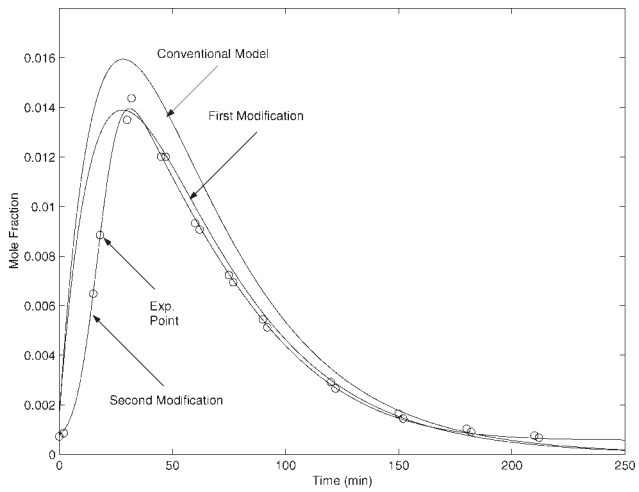

Figure 17. Modified predictions for the third depressurization step (1100–200 kPa).

simply extending the operating time. This is consistent with the industrial and experimental observations in CBM and ECBM practice.

4. Physical explanations for adjusting parameters to fit the dynamic experimental and simulation results better have been suggested. Although further justification is necessary, these observations may have significant implications in industrial applications. The incorporation of an adjustable term in the classical diffusion equation potentially permits tailoring of porous materials by adjusting contributions from diffusion and directional forces. Depending on the requirements of different industrial applications, such as gas separation and storage, optimal configurations of CNTs might be determined using system optimization techniques.

The following four recommendations are made for future work.

1. Incorporation of the rigorous potential gradient functions rather than empirical representations into models for complex porous media, such as coals and activated carbons with very high heterogeneity. The real challenge is related to the characterization of the potential fields, which requires more complete knowledge on the structures and chemical compositions of these porous media.

2. Experimental validation of the models developed in this work for molecular transport through cone- and double cone-shaped CNTs, and Li^+ doped pores. This requires manufacture of nanopores with desired characteristics (size and morphology), and improved measurement techniques.

3. CO_2 is a polar molecule with static dipole polarizability $\alpha_p = 2.594 \times 10^{-24}$ cm^3, and quadrupole moment as $Q_{zz} = -4.3 \times 10^{-26}$ erg$^{1/2}$ cm$^{5/2}$, so interactions between electrical charges need to be properly accounted for. As a prelude of the study on charge interactions, functional group distributions on nanopore surfaces should be determined. A thorough study on interactions between polar molecules and polar functional groups is a very important yet underdeveloped research area.

4. As shown by the authors and Chan et al., the connectivity and tortuosity in real materials is an important issue[4,20] requiring further theoretical and experimental studies.[21]

Notation

$\mathbf{A}$ = orthogonal collocation matrix for the first order spatial derivative, dimensionless.
$\mathbf{B}$ = orthogonal collocation matrix for the second order spatial derivative, dimensionless.
B_μ = nanopore permeability, mol/(m s Pa).
b = parameter in Toth isotherm equation, 1/Pa.
C = gas phase concentration, mol/m^3.
c = parameter for the characterization of linear potential fields, J/m.
D = diffusion coefficient, m^2/s.
D_{DR} = diffuse reflection diffusivity, m^2/s.
D_p = pore diameter in CNT, m.
E = random fluctuation force, N.
$\mathbf{F}$ = directional force vector, N.
F = hypergeometric function.
f = number or molar density, 1/m^3 or mol/m^3.
f_d = pore-size distribution, m/(kg m).
J = molar flux, mol/(m^2 s).
K = permeability, m^2.
k_A = Avogadro constant, 1/mol.
k_B = Boltzmann constant, J/K.
k_{sf} = solid–fluid binary interaction parameter, dimensionless.
L = length of the pore, m.
m = mass of molecule, kg.
N = number of molecules in the system, dimensionless.
n = number or mole of particle added to the system, dimensionless or mol.
P = gas phase pressure, N/m^2 or Pa.
P_μ = pressure surrounding nanopores, N/m^2.
Q_{zz} = quadrupole moment, erg$^{1/2}$ cm$^{5/2}$.
q = pseudo velocity defined as $q = D\beta c$, m/s.
R = radius of cylindrical pores, m.
R_g = ideal gas constant, J/(K mol).
r = distance of the molecule in cylindrical pore from the origin, m.
T = temperature, K.
t = time variable, s.
t_o = parameter in Toth isotherm equation, dimensionless.
U = potential energy, J/mol.
U_0 = minimum interaction energy, J/mol.
v = axial velocity, m/s.
w = half width of slit shaped pores, m.
x = axial position, m.
$\mathbf{x}$ = spatial position vector, m.
y = pseudo spatial coordinate defined as $y = x + qt$, m.
z = distance from the central plane to the centre of the first layer of wall atoms in slit pores, m.

Greek letters

α = Maxwell coefficient to account for surface roughness, dimensionless.
α = empirical parameter for estimation of velocity, dimensionless.
α_p = Dipole polarizability, cm^3.
β = parameter defined as $\beta = 1/(k_B T)$, 1/J.
δ = Dirac delta function.
Δ = spacing of lattice layers, m.
γ = fractional coefficient, kg/s.
ρ_p = solid density, kg/m^3.
ρ_s = number of lattice atoms per unit volume, 1/m^3.
$\hat{\rho}$ = average gas density, mol/m^3.
σ = amplitude of random fluctuating force, dimensionless.
σ_i = diameter of particle i, m.
σ_{ij} = effective diameter for the particle pair $\{i, j\}$, m.
ε_i = characteristic energy of particle i, J.
ε_{ij} = cross potential well depth for the particle pair $\{i, j\}$, J.
ζ = parameter defined as $\zeta = r/R$ in the hypergeometric function, dimensionless.
μ = viscosity, (N s)/m^2.
ν = dummy independent variable in integral functions.
λ = half distance between two fractures, m.
τ = tortuosity, dimensionless.
τ_μ = nanopore tortuosity.

Subscripts

C = convection.
D = diffusion.
e = effective.
i = component i.
m = mean value.
μ = nanopores.

Literature Cited

1. Einstein A. *Investigations on the Theory of the Brownian Movement*. Edited with notes by Furth R, Translated by Cowper AD, New York: Dover, 1956.
2. Do DD. *Adsorption Analysis: Equilibria and Kinetics*. London: Imperial College Press, 1999.
3. Bhatia SK, Chan HB, Sholl DS. Comparison of diffusive and viscous contributions to transport coefficients of light gases in single-walled carbon nanotubes. *Mol Simul*. 2005;31:643–649.
4. Wang FY, Zhu ZH, Rudolph V. Molecular transport in nanopores with broad pore-size distribution. *AIChE J*. 2008;54:2009–2023.
5. Jepps OG, Bhatia SK, Searles DJ. Modelling molecular transport in slit pores. *J Chem Phys*. 2004;120:5396–5406.

6. Aranovich GL, Donhue MD. Limitations and generalization of the classical phenomenological model for diffusion in fluids. *Mol Phys*. 2007;105:1085–1093.
7. Wang FY, Zhu ZH, Massarotto P, Rudolph V. A simplified dynamic model for accelerated methane residual recovery from deep coals. *Chem Eng Sci*. 2007;62:3268–3275.
8. Wang FY, Zhu ZH, Massarotto P, Rudolph V. Mass transfer in coal seams for CO_2 sequestration. *AIChE J*. 2007;53:1028–1049.
9. Bae JS, Bhatia SK. High-pressure adsorption of methane and carbon dioxide on coal. *Energy Fuels*. 2006;20:2599–2607.
10. Schulten K, Kosztin I. *Lectures in Theoretical Biophysics*. University of Illinois at Urbana-Champaign, 2000. Available at: http://www.ks.uiuc.edu/~kosztin/PHYCS498NSM/
11. Friedlander SK. *Smoke, Dust, and Haze: Fundamentals of Aerosol Dynamics*, 2nd ed. New York: Oxford University Press, 2000.
12. Steele WA. *The Interaction of Gases with Solid Surface*. Oxford: Pergamon, 1974.
13. Rao MB, Jenkins RG, Steele WA. Potential functions for diffusion in carbon molecular sieves. *Langmuir*. 1985;1:137–141.
14. Do DD, Do HD. Adsorption of carbon tetrachloride on graphitized carbon black and in slit graphitic pores: five-site versus one-site potential models. *J Phys Chem B*. 2006;110:9520–9528.
15. Do DD, Do HD. Adsorption of benzene on graphitized carbon black: reduction of the quadrupole moment in the adsorbed phase. *Langmuir*. 2006;22:1121–1128.
16. Zhang XR, Wang WC, Jiang GF. A potential model for interaction between the Lennard-Jones cylindrical wall and fluid molecules. *Fluid Phase Equilib*. 2004;218:239–246.
17. Villadsen J, Michelsen ML. *Solution of Differential Equation Models by Polynomial Approximation*. Englewood Cliffs: Prentice-Hall, 1978.
18. Finlayson BA. *The Method of Weighted Residuals and Variational Principles: With Applications in Fluid Mechanics, Heat and Mass Transfer*. New York: Academic Press, 1972.
19. Chen H, Sholl DS. Prediction of selectivity and flux for CH_4/H_2 separations using single walled carbon nanotubes as membranes. *J Membr Sci*. 2006;269:152–160.
20. Chan F, Mourhatch R, Tsotsis TT, Sahimi M. Pore network model of transport and separation of binary gas mixture in nanoporous membranes. *J Membr Sci*. 2008;315:48–57.
21. Hunt A. *Percolation Theory for Flow in Porous Media*. Berlin: Springer, 2005.

Appendix A: Derivation of Smoluchowski Diffusion Equation

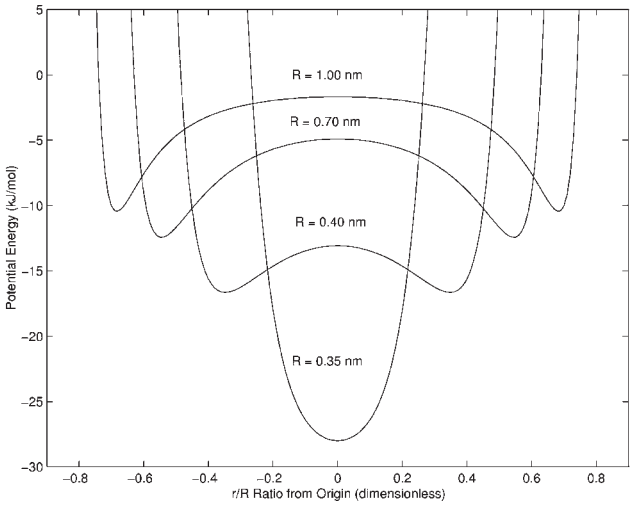

Figure B1. Potential energy profiles of CO_2 in cylindrical CNT with various sizes.

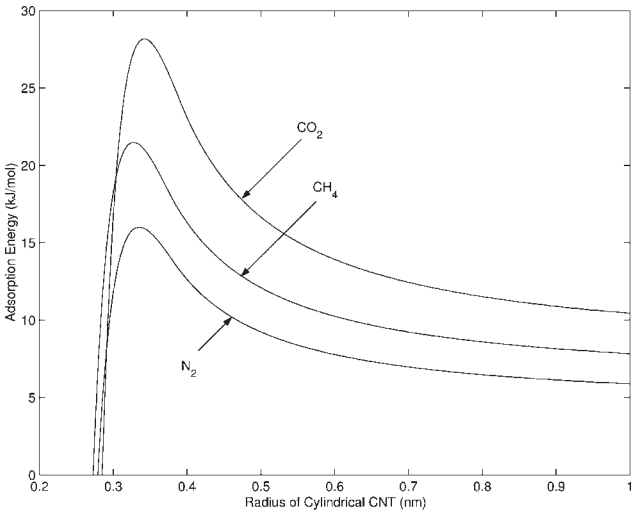

Figure B2. Adsorption energy profiles for CO_2, CH_4, and N_2.

The Boltzmann distribution $\exp[-\beta U(x)]$, $\beta = 1/(k_B T)$ is postulated as a stationary solution to the Fokker-Planck diffusion equation described by Eq. (11), that is:

$$\frac{\partial}{\partial t} f = \left(\nabla^2 D - \nabla \cdot \frac{\mathbf{F}}{\gamma} \right) f = 0 \qquad f = \exp[-\beta U(x)] \tag{A1}$$

In this case, it can be shown that the variable diffusivity satisfies the following relationship:

$$\nabla D = \mathbf{F}(\mathbf{x}) \left(\frac{1}{\gamma} - D\beta \right) \tag{A2}$$

Through differential operations, we obtain:

$$\begin{aligned} \nabla \cdot [\nabla D f] &= \nabla \cdot [D \nabla f] + \nabla \cdot [f \nabla D] \\ &= \nabla \cdot [D \nabla f] + \nabla \cdot \left[\mathbf{F}(\mathbf{x}) \left(\frac{1}{\gamma} - D\beta \right) f \right] \\ &= \nabla \cdot [D \nabla f] + \nabla \cdot [D\beta f] + \nabla \cdot \left[\frac{\mathbf{F}(\mathbf{x})}{\gamma} f \right] \end{aligned} \tag{A3}$$

Substituting Eq. (A3) into Eq. (11), the Fokker-Planck diffusion equation is converted to the Smoluchowski diffusion equation represented by Eq. (13).

Appendix B: Potential Energy and Adsorption Energy Profiles

The potential energy profiles for CO_2 molecules in cylindrical CNTs with various pore sizes are shown in Figure B1.

The adsorption energy profiles for three gases, namely CO_2, CH_4, and N_2 are depicted in Figure B2.

Manuscript received Apr. 10, 2008, and revision received Oct. 9, 2008.